First-principles study of ultrathin magnetic Mn films on W surfaces. I. Structure and magnetism

S. Dennler* and J. Hafner
Institut für Materialphysik and Center for Computational Materials Science, Universität Wien, Sensengasse 8, A-1090 Wien, Austria
(Received 22 July 2005; revised manuscript received 30 September 2005; published 9 December 2005)

The structural and magnetic properties of static compact thin Mn films deposed on W(100) and W(110) substrates have been investigated in the framework of the density functional theory. In good agreement with experiments, pseudomorphically adsorbed Mn films up to three monolayers (ML) are found to be stable despite the huge tensile strain induced by the epitaxial conditions. For Mn/W(110) our results demonstrate a $c(2\times2)$ in-plane antiferromagnetic order for thicknesses up to 3 ML, with a degenerated layered antiferromagnetism in the (110) planes for 3 ML thick Mn/W(110) films. For Mn/W(110) our calculations predict a ferromagnetic arrangement in 1 and 2 ML thick films stabilized by the hybridization with the substrate, with a transition to an antiferromagnetism layered in (100) planes at higher thickness. The effects induced by the reduced dimensionality are discussed based on the comparison with bulk Mn and free-standing Mn ML. The magnetic contribution to the adsorption is determined by comparing magnetic and nonmagnetic calculations.

DOI: 10.1103/PhysRevB.72.214413 PACS number(s): 75.70.Ak, 68.43.Bc, 68.60.−p

I. INTRODUCTION

Magnetism on the nanoscale is one of the current research frontiers in magnetism. The aim is to understand the physical principles governing the properties of complex multicomponent nanostructures and to use this knowledge for the design of components for data-storage devices or in the up-coming magnetoelectronics (or "spintronics").[1] Driven by the desire to apply the exchange-bias effect[2] to tune the characteristics of giant-magnetoresistance devices, important efforts are currently devoted to studying antiferromagnetic thin films adjacent to ferromagnetic or nonmagnetic films or substrates.[3,4] Fe/Cr multilayers have been studied extensively (see, e.g., the paper by Pierce *et al.* in Ref. 1 and the review by Zabel[5]), with particular attention to the modification of the antiferromagnetic spin-density-wave structure of bulk body-centered-cubic Cr imposed by the film geometry and exchange interactions across the Fe/Cr interface.

For Mn, the structure-property relationship is even more complex. Depending on temperature and pressure, Mn exists in five allotropic forms.[6–8] α-Mn has a complex body-centered-cubic structure with 58 atoms per cubic cell, it is stable up to temperatures of 1000 K and pressures of about 165 GPa. Below $T_N=95$ K α-Mn adopts a noncollinear antiferromagnetic structure, the paramagnetic-antiferromagnetic transitions is coupled to a tetragonal distortion of the crystal structure. Under pressure, α-Mn transforms to a nonmagnetic hexagonal-close-packed phase. β-Mn (stable between 1000 K and 1368 K) is simple cubic with 20 atoms per cell. A face-centered-cubic (fcc) γ-phase exists between 1368 K and 1406 K, a body-centered-cubic δ-Mn phase from 1406 K up to the melting point of $T_M=1517$ K. The magnetic properties of the high-temperature phases may be studied on quenched samples, by extrapolating data acquired on Mn alloys to zero impurity concentration, or in thin films stabilized by epitaxial growth. From a study of dilute alloys of Fe in Mn, Endo and Ishikawa[9] concluded that γ-Mn is antiferromagnetic with a Néel temperature of $T_N=570$ K and a magnetic moment of $2.3\mu_B$. The formation of a layered antiferromagnetic order on (001) planes is coupled to a tetragonal distortion with $(c/a)_{\mathrm{fct}}=0.946$ relative to the fcc structure. First-principles density-functional calculations[10,11] correctly reproduce the tetragonal distortion, but predict somewhat smaller magnetic moments. In addition, a metastable tetragonally expanded phase $[(c/a)_{\mathrm{fct}}>1]$ with $c(2\times2)$ in-plane antiferromagnetism has been predicted. While for γ-Mn theory and experiment are in reasonable agreement, magnetism in δ-Mn is found to be much more complex. Earlier density-functional calculations find δ-Mn to be ferromagnetic at equilibrium, and a transition to a layered antiferromagnetic configuration in an expanded state,[12–14] while more recent studies have demonstrated that the magnetic ground state has $c(2\times2)$ antiferromagnetic order in (001) planes[8,11] and that again the appearance of antiferromagnetism is coupled to a tetragonal distortion of the lattice [axial ratio $(c/a)_{\mathrm{fct}}=0.684$ or $(c/a)_{\mathrm{bct}}=0.967$]. For a detailed discussion of the magnetic properties of the tetragonal phases of Mn over a wide range of tetragonal distortions, we refer to the recent work of Spišák and Hafner[11] and to further references given therein.

Ultrathin films of Mn with a tetragonal structure have been grown on a number of fcc (Al, Cu, Ni, Pd, Ir)[15–20] and bcc (Fe, V, W, Fe-Mn, Cr-Mn).[21–28] Mn-films grown at low temperature on the surfaces of noble and late transition metals show a tetragonally expanded fct structure close to γ-Mn, $c(2\times2)$ in-plane antiferromagnetism (AF) in the monolayer limit and layered AF in thicker films, high-temperature deposition or annealing leads to interdiffusion and the formation of $c(2\times2)$ surface alloys.[17,18] Surface alloying and a ferromagnetic coupling between the Mn atoms in the alloy layer are in good agreement with *ab initio* calculations.[17,29,30]

The proximity of Mn to Fe in the Periodic Table has led to the expectation that δ-Mn could possibly share similar magnetic properties with α-Fe, and hence many efforts have been spent on attempts to grow thin films of Mn with a bcc structure. Ultrathin Mn/Fe(100) films have been investigated most extensively.[11,21–23] The unavoidable frustration of the exchange interactions at the interface between a ferromagnetic and an antiferromagnetic material adds to the complexity of the structure-property relationship of the tetragonal

phases of Mn. The experimental and theoretical results reported so far are highly controversial, a summary of past work and *ab initio* calculations have been presented very recently by Spišák and Hafner.[11] The results demonstrated that the extraordinary complexity of Mn/Fe(100) films arises from the competition between the the intrinsic $c(2\times2)$ in-plane antiferromagnetism of δ-Mn which dominates at the free surface and the layered antiferromagnetism in the deeper layers imposed by the coupling with the ferromagnetic substrate.

Therefore, for a better understanding of the intrinsic properties of thin δ-Mn films the investigation of overlayers grown on nonmagnetic bcc substrates remains of great interest. Tian *et al.*[24,28] have investigated the growth of Mn films on V(100) and W(100) surfaces using low-energy electron diffraction (LEED) and *ab initio* DFT methods. Tungsten is considered to be a particularly promising substrate material because the high melting point and the large difference in the surface energies of W and Mn should largely suppress interdiffusion. Tian *et al.* argued, on the basis of DFT calculations by Qiu *et al.*,[31] that the misfit to the substrate is much smaller for δ than for γ-Mn, the LEED data demonstrate that the structure of the Mn films corresponds essentially to a tetragonally contracted bcc structure, $(c/a)_{\mathrm{bct}}=0.966$ on V(100), and $(c/a)_{\mathrm{bct}}=0.897$ on W(100). However, no experimental characterization of the magnetic structure of the films is available, and the DFT calculations assumed *a priori* a layered antiferromagnetic structure and a large fixed atomic volume ($V_{\mathrm{at}}=12.94$ Å^3) for tetragonal Mn based on extrapolations of the structure data on Fe-Mn alloys,[9] which is by far larger than the equilibrium volume resulting from any first-principles calculation. If these values are used, a much larger misfit (about 13%) is calculated.

Very recently several experimental studies have demonstrated the possibility of stabilizing thin films of δ-Mn on bcc W(110) surfaces up to several layers[25–28] despite the tensile strain induced by the large misfit. The work on Mn/W films was motivated to a large extent by the successful preparation of pseudomorphic Fe, Co, and Fe-Co layers on W(110) substrates.[32–35] The results of these studies are remarkable from several aspects: (i) Fe/W(100) and Co/W(110) monolayers have been characterized as "magnetically dead" on the basis of magneto-optic Kerr effect measurements,[36,37] while *ab initio* spin-density functional calculations[38,39] demonstrated that they are indeed antiferromagnetic, in contrast to the ferromagnetism of bulk Fe and Co. In the case of Fe/W(100) the theoretical prediction has recently received an experimental confirmation.[40] (ii) The pseudomorphic relationship extends only to coverages barely exceeding the monolayer limit, in Co/W(110) a denser phase with partial dislocations already before the first monolayer is completed, for Fe/W(110) layers the transition to a denser structure begin at about 1.2 monolayers. (iii) The theoretical studies show that a strong adsorbate-substrate hybridization at the interfaces is essential for stabilizing the pseudomorphic relationship, but also for the profound modification of the magnetic properties relative to the bulk material.

For pseudomorphic Mn/W(110) films in-plane $c(2\times2)$ antiferromagnetism has been reported for monolayer films.[26] The epitaxial relationship is maintained up to a coverage of about three monolayers,[25] but in contrast to Fe/W(110) films, already the first Mn layer exhibits a modest growth anisotropy in the [001] direction. This anisotropy becomes even much more pronounced in the second Mn layer, and for films with three and more monolayers, island growth is observed. Very recent work has extended the investigation to $\mathrm{Fe}_x\mathrm{Mn}_{1-x}$ alloy monolayers on W(110).[41] The Curie temperature of the alloy monolayers drops to zero if the Mn concentration exceeds 30%, LEED data confirm a pseudomorphic relationship. The aim of the present work is to explore the structural and magnetic properties of ultrathin Mn films adsorbed on W surfaces. Our approach is based on density functional theory, we show how such atomistic first-principles modeling and simulation can fruitfully supplement the experiments to get quantitative parameters such as atomic magnetic moments that are generally difficult to determine experimentally. We also take benefit of computer experiments to evaluate the effects of the reduced dimensionality from the comparison of the thin adsorbed films to free-standing ML and bulk δ Mn. Our study is focused on W(110) as well as W(100) for which to our knowledge there has been no experimental investigation of the magnetic properties yet. The paper is organized as follows. In Sec. II we present our computational approach. Section III presents some reference results for the clean W surfaces, bulk δ Mn and free-standing ML, and Sec. IV describes our results for thin Mn/W(110) and Mn/W(100) films up to three layers. Finally, Sec. V summarizes our results and points to future developments.

II. COMPUTATIONAL DETAILS

Our calculations were carried out within the density functional framework (DFT) using the Vienna *ab initio* simulation package (VASP)[42,43] implementing the projector-augmented wave (PAW) method.[44,45] The plane-wave basis set contained components with energies up to 280 eV while the Brillouin zone was sampled using Monkhorst-Pack meshes of k-points[46] adapted to the size of the computational cell. These parameters were carefully checked to give reasonably accurate results, as it is demonstrated by the good agreement obtained for bulk Mn and clean W surfaces both with other *ab initio* calculations and with experiments (see below). The influence of nonlocal corrections in the exchange-correlation functional has been already largely investigated in the literature.[47,48] In particular, earlier calculations have demonstrated that the use of the generalized gradient approximation (GGA) is mandatory to describe correctly the properties of magnetic Mn.[11,29] Here the GGA functional proposed by Perdew, Burke, and Ernzerhof (PBE)[49] was employed. The corresponding value for the tungsten lattice constant, $a_{\mathrm{W}}=3.171$ Å, agrees very well with the experimental value[50] $a_{\mathrm{W}}=3.165$ Å, slightly better than the value obtained with the GGA functional of Perdew and Wang (PW91),[51] $a_{\mathrm{W}}=3.181$ Å, in a previous study of thin Fe/W films.[39] On the other hand, a too small lattice constant of 3.133 Å is found within the local density approximation (LDA).

For the Brillouin-zone integrations, a Monkhorst-Pack mesh equivalent to a $12\times12\times12$ grid for the primitive

TABLE I. Lateral displacements along the ⟨110⟩ direction (s_i in Å) and vertical interlayer relaxations ($\delta_{i/j}$ in %) for the atomic layers i,j in the fully relaxed clean W(110) and W(100) surfaces. E_{rlx} and E_{rec} are the energy gains (in meV/surface atom) upon relaxation of the ideal surface and upon reconstruction, respectively.

	W(110)		W(100)			
	This work	PAW-PW91[a]	This work	PAW-PW91[a]	LAPW-LDA[b]	Expt.[c]
s_1	0.00	0.00	0.27	0.27	0.27	0.24±0.025
s_2	0.00	0.00	0.04	0.04	0.05	0.046±0.016
s_3	0.00	0.00	0.01	0.01	0.02	
$\delta_{1/2}$	−4.6	−4.7	−9.7	−7.8	−6.0	−4±10
$\delta_{2/3}$	0.5	0.2	2.6	0.5	0.5	
$\delta_{3/4}$	−0.3	−0.6	−0.8	−0.5		
E_{rlx}	39		199			
E_{rec}			64	60	110	

[a]Reference 39.
[b]Reference 54.
[c]Reference 53.

cubic cell used in the bulk calculations was employed. To model the clean and Mn-covered W surfaces, a standard slab configuration was used, with periodically repeated supercells separated by a vacuum layer of about 14 Å. Convergence of the calculations with respect to the thickness of the slab and of the vacuum layer has been carefully tested to provide a good compromise between accuracy and computational tractability. The substrate was modeled with six W layers, of which three layers at the bottom were kept fixed in bulklike positions with the calculated tungsten lattice constant, and Brillouin-zone integrations were performed on two-dimensional Monkhorst-Pack meshes corresponding to $12\times12\times1$ and $14\times12\times1$ grids for the primitive (100) and (110) surface unit cells, respectively. In the following, the different layers are referred to by their index being counted from the Mn/W interface, with indexes 1, 2, 3,… for the W layers and I, II, III,… for the Mn ones.

The geometric relaxation was performed with a quasi-Newton algorithm using the exact Hellmann-Feynman forces, with a criterion for stopping the structural optimization of 0.01 eV/Å. To speed up convergence, we employed a Methfessel-Paxton smearing with a width of 0.1 eV. Unless stated explicitly, the calculations take into account magnetism through a spin-polarized DFT approach. The spin interpolation formula of Vosko, Wilk, and Nusair which is known to give reasonable results was used.[52] Local magnetic moments were calculated by integrating the magnetization densities within atom-centered spheres with radii of 1.373 Å, corresponding to touching spheres in bulk tungsten. Finally, this computational setup introduces a numerical error in the adsorption energies that can be estimated to a few meV. As it will be demonstrated below, this allows to determine undoubtedly the most favorable configurations.

III. CLEAN W SUBSTRATE, δ bcc Mn BULK AND FREE-STANDING Mn MONOLAYERS

A. Clean W(110) and W(100) surfaces

As a further test of the accuracy of our calculations, we first present in Table I our results for the nonmagnetic clean tungsten surfaces. The excellent agreement obtained both with previous *ab initio* calculations and with experiments supports the reliability of our computational setup. The case of the W(100) surface is particularly interesting since it is known to exhibit a $(\sqrt{2}\times\sqrt{2})R45°$ reconstruction at low temperature[53] as illustrated in Fig. 1(a). The energy gain upon relaxation of the ideal (1×1) W(100) surface from the rigid configuration with bulklike fixed interatomic distances is quite important ($E_{\mathrm{rlx}}=199$ meV/surface atom). As observed in experiment the ideal surface turns out to be unstable towards reconstruction leading to a further stabilization by $E_{\mathrm{rec}}=64$ meV/surface atom. In good agreement with the experimental measurements and previous calculations we determine a displacement of ±0.27 Å along the ⟨110⟩ direction in the top surface layer and similar, but strongly damped displacements in the deeper layers. This supports the hypothesis often made in the interpretation of experimental data to assume that the reconstruction affects only the two uppermost surface layers. However, it will be shown in Sec. IV A that the surface reconstruction locally vanishes upon adsorption of a Mn atom. Therefore, without further specification we will consider in the following only nonreconstructed W(100) surfaces.

Note that our results using the PBE functional are very close to those obtained with the PW91 functional[51] in a previous study using the same code.[39] This demonstrates here

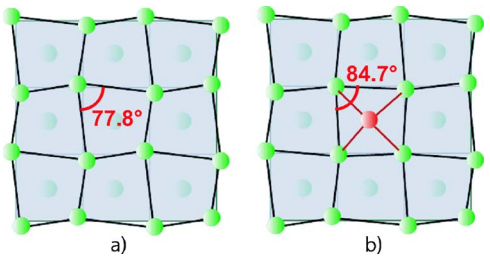

FIG. 1. (Color online) (a) $(\sqrt{2}\times\sqrt{2})R45°$ reconstruction of the clean W(100) surface. (b) Local reduction of the reconstruction upon adsorption of a Mn atom.

TABLE II. Relative energy ΔE (in meV/Mn), atomic magnetic moment μ (in μ_B/Mn), structural parameters a and c (in Å), c/a ratio, atomic volume V_{at} (in units of V_{at}^0=11.091 Å^3/atom calculated for the fully relaxed bcc Mn phase with the AF1 order), interlayer spacings d_{100} and d_{110} (in Å) for different geometries of bulk δ bcc Mn and different magnetic orders, as obtained from fully *ab initio* calculations. Note that for Mn matching the W(110) surface, we do not indicate a and c since the relaxed unit cell is not tetragonal anymore.

Geometry of bulk δ Mn	Magnetic order	Δ_E	μ	a	c	c/a	V_{at}	d_{100}	d_{110}
Fully relaxed	AF1	0	±1.44	2.840	2.750	0.968	1.000	1.375/1.420	1.944/2.008
	AF2					unstable			
	FM	27	0.86	2.786	2.786	1.000	0.975	1.393	1.970
	NM	52	0.00	2.760	2.760	1.000	0.948	1.380	1.952
Isostructural to bcc W	AF1	371	±3.40	3.171	3.171	1.000	1.437	1.586	2.242
	AF2	253	±3.52	3.171	3.171	1.000	1.437	1.586	2.242
	FM	586	3.53	3.171	3.171	1.000	1.437	1.586	2.242
	NM	1105	0.00	3.171	3.171	1.000	1.437	1.586	2.242
Matching the W(100) surface	AF1	183	±2.01	3.171	2.536	0.800	1.150	1.268	
	AF2	76	±2.61	3.171	2.536	0.800	1.150	1.268	
	FM	249	1.28	3.171	2.536	0.800	1.150	1.279	
Matching the W(110) surface	AF1	141	±2.84				1.169		1.823
	AF2	183	±2.56				1.169		1.823
	FM	280	1.21				1.093		1.704

the small influence of the GGA version used to approximate the exchange and correlation energy functional, whereas on the other hand, the LDA significantly overestimates the reconstruction energy.

In contrast to the W(100) surface, the W(110) surface does not show any reconstruction. As expected for metallic surfaces, due to the higher compacity and lower corrugation the vertical interlayer relaxations are much smaller than for the more open W(100) surface. Consequently the energy gain upon relaxation (E_{rlx}=39 meV/surface atom) is also lower.

B. Bulk δ bcc Mn

Since in the following we will be dealing with thin Mn films, it seems natural to consider first the bulk material. Therefore, we now present results for bulk δ-Mn close to a bcc geometry that will later serve as reference calculations (obtained within the same computational framework) to estimate the influence of the reduced dimensionality on the magnetic properties of free-standing and adsorbed Mn layers. The results are compiled in Table II. We considered two AF configurations which are depicted in Fig. 2, (i) in-plane $c(2\times2)$ antiferromagnetism in (100) planes (AF1), and (ii) a layered antiferromagnetism in (100) planes (AF2).

The ground state is a slightly distorted body-centered-tetragonal (bct) structure (axial ratio c/a=0.968) with AF1 order, while AF2 is found to be unstable. The magnetic moment is $\mu=1.44\mu_B$ and the atomic volume V_{at}^0 =11.091 Å^3/atom. Our results are in very good agreement with a recent investigation of magnetism in tetragonal Mn (Ref. 11) performed with the same computational approach but with the PW91 functional (c/a=0.967, $\mu=1.42\mu_B$, V_{at}^0 =11.13 Å^3/atom). This stresses once again that the PW91 and PBE functionals lead to very similar results. A metastable FM solution less stable by ΔE=27 meV/atom has a smaller moment ($\mu=0.86\mu_B$/atom) and a ideal bcc structure (c/a=1.000). The NM structure is disfavored with ΔE =52 meV/atom and exhibits an atomic volume 5.2% smaller than the ground-state AF1 geometry.

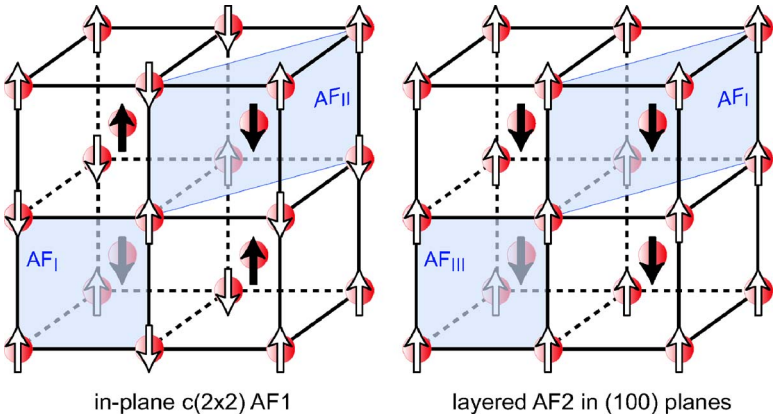

FIG. 2. (Color online) Schematic illustration of the different antiferromagnetic (AF) configurations considered in our study of bcc δ-Mn. The colored panels and the corresponding labels indicate the notations that we use to describe the different magnetic structures for Mn films adsorbed on W(110) and W(100) substrates (see Fig. 3).

TABLE III. Relative total energy ΔE (in eV/atom), atomic magnetic moment μ(Mn) (in μ_B/atom) and lattice constant a of free-standing Mn(100) and Mn(110) ML with different magnetic structures. The energy differences ΔE are calculated with respect to the most stable configuration of each geometry. The notations NM, FM, AF_I, and AF_{II} stand for the nonmagnetic, ferromagnetic, and the $c(2\times2)$ and $p(2\times1)$ in-plane antiferromagnetic structures, respectively.

		Homothetical relaxation			a=3.171 Å	
		ΔE	μ(Mn)	a	ΔE	μ(Mn)
Mn(100)	AF_I	0.000	2.55	2.24	0.862	4.35
	AF_{II}				0.902	4.30
	FM-LS	0.638	0.12	2.10	0.920	4.31
	FM-HS	0.399	3.95	2.60		
	NM	0.293		2.12	3.860	
Mn(110)	AF_I	0.000	3.30	2.80	0.239	3.99
	AF_{II}				0.302	4.04
	FM-LS	0.421	1.52	2.60	0.459	4.02
	FM-HS	0.426	3.86	3.00		
	NM	0.509		2.51	2.178	

Since we are interested in this paper in thin Mn films adsorbed on W surfaces, it is instructive to consider more carefully the properties of strained bulk δ bcc Mn matching the W(110) or the W(100) surfaces. The expansion to an ideal bcc structure with the same lattice constant as W, $a=c=a_W=3.171$ Å, corresponds to a large increase of the atomic volume (more than 43%) and consequently results in a strong enhancement of the moments ($\mu \approx 3.4$–$3.5\mu_B$/atom) in all magnetic phases, short of the Hund's-rule limit of $5\mu_B$. This is accompanied by a significant stabilization of the magnetic solutions with respect to the nonmagnetic one which is less stable by 0.52 to 0.85 eV/atom. Remarkably our results demonstrate a change in their relative stabilities, at such a dilated geometry the AF2 structure is the most stable with a large moment of $\mu=3.52\mu_B$/atom. The energy needed to expand the structure from the ground state, including the change of magnetic order, amounts to 253 meV/atom. An AF1 solution is found 118 meV/atom above the AF2 one, a FM phase exists but is much less stable (333 meV/atom above the AF2 one).

We now consider more specifically a bct Mn crystal whose in-plane lattice constant in the (110) and (100) planes, respectively, is constrained to the lattice parameter of bcc W ($a_W=3.171$ Å) while the interlayer spacings d_{100} and d_{110} in the perpendicular direction are relaxed. Starting from bulk Mn isostructural to bcc W, the corresponding relaxation allows a strong decrease of the atomic volume towards its ground state value and this results in significantly lower energy differences ΔE with respect to the AF1 ground state. For both (100) and (110) matching surfaces, the FM solutions appear to be quite unfavorable with a high energy difference of $\Delta E_{100}=249$ meV/atom and $\Delta E_{110}=280$ meV/atom. Even if both AF1 and AF2 solutions have almost the same geometric properties (same $d_{100}=1.268$ Å, $d_{110}=1.823$ Å), their energetical and magnetic properties depend strongly on the in-plane constraints, for Mn matching W(100) the most stable phase is AF2 with a low energy difference of $\Delta E_{100}=76$ meV/atom and a large magnetic moment of $\mu=2.61\mu_B$/atom while the AF1 solution is found to be 107 meV/atom above the ground state with a smaller $\mu=2.01\mu_B$/atom. On the other hand, for Mn matching W(110) the AF1 phase is found more stable by 42 meV/atom than the AF2 one. The energy difference relative to the fully relaxed ground state of Mn with AF1 order is, however, twice as large as for Mn matching W(100), $\Delta E_{110}=141$ meV/atom. The atomic magnetic moment $\mu=2.84\mu_B$/atom is also quite high.

Assuming volume conservation relative to the AF1 ground state of bcc δ-Mn ($V^0_{at}=11.091$ Å^3/atom) we estimate much lower interlayer spacings of $d_{110}=1.56$ Å and $d_{100}=1.10$ Å. This demonstrates that due to a strong magnetovolume effect the enhanced magnetic moments are coupled to a strong expansion of the interlayer distances.

C. Free-standing Mn(110) and Mn(100) monolayers

Having characterized the uncovered W(100) and W(110) surfaces as well as the bulk bcc Mn material, the next step is naturally the study of free-standing Mn(100) and Mn monolayers (ML) in view of their epitaxial adsorption on a tungsten substrate. This will allow later to evaluate the strength of adlayer-substrate hybridization, and the resulting effects on the possible magnetic configurations within the Mn film.

Figure 4 illustrates the relative stability of Mn(100) and Mn(110) ML with different magnetic structures, as well as the corresponding atomic magnetic moments, as a function of the lattice constant. Since our aim is to study the adsorption of a ML on W(100) and W(110) substrates, the lattice constant a was varied by homogeneous expansions or contractions, keeping the (100) or (110) geometry fixed. The figure is complemented by Table III which details the results for the most stable configurations and for those constrained to a lattice constant matching that of bulk tungsten. We have considered several possible spin structures for the Mn ML, which are schematically depicted in Fig. 3: (i) ferromagnetic (FM), (ii) antiferromagnetic $c(2\times2)(AF_I)$ with an antiferro-

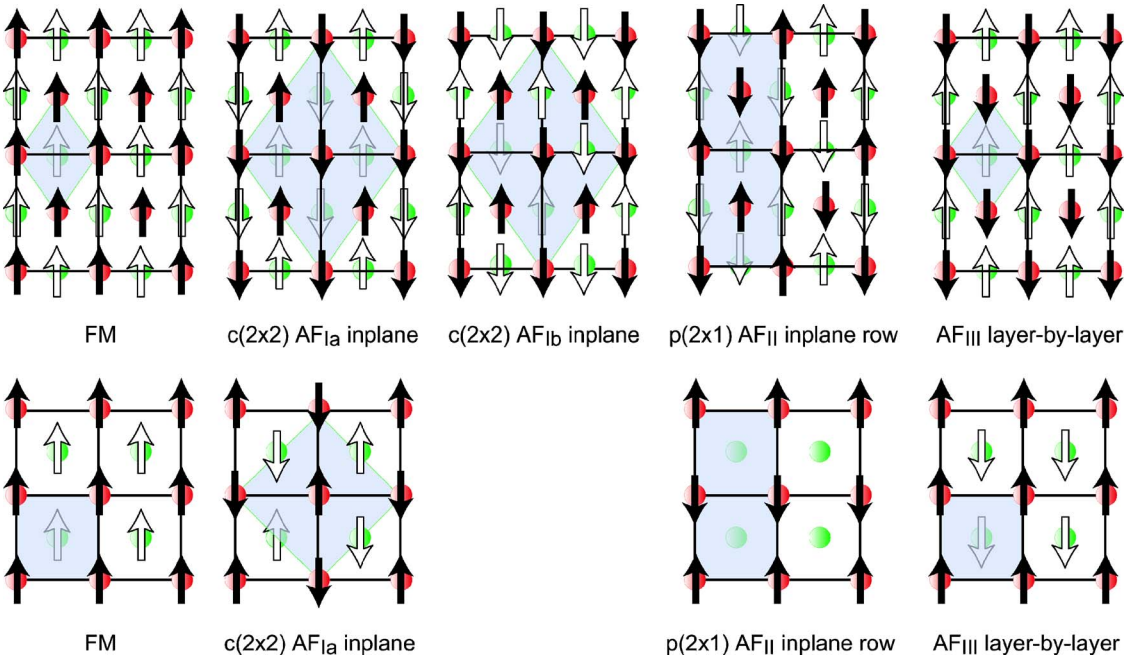

FIG. 3. (Color online) Schematic illustration of the different magnetic orders considered in our study for the pseudomorphic growth of thin Mn films on W(110) (top) and W(100) (bottom). The indices a and b refer to the slightly different magnetic arrangements that can exist for films containing more than 1 ML. The corresponding unit cells are indicated by shaded areas.

magnetic coupling between all nearest-neighbor atoms, and (iii) antiferromagnetic $p(2\times1)(\mathrm{AF_{II}})$, where two nearest-neighbor atoms couple ferromagnetically and the other two couple antiferromagnetically. The link with the AF arrangements that we considered in our study of δ-Mn in the preceding section is detailed in Fig. 2.

From a general point of view the comparison of the results for both (100) and (110) geometries in connection with those for bulk δ Mn reveals the usual trends in structure, magnetism, and stability that essentially result from the different effective coordination numbers. The transition from a bulk phase to a two-dimensional film geometry results in significantly increased magnetic moments as the result of the reduced coordination. Moreover, as a consequence of the higher atomic coordination within the (110) ML (four neighbors at $a\sqrt{3}/2$ plus two at a) the optimal lattice constant a for a given magnetic state is found to be larger for the (110) ML (by typically 15%–25%) compared to the (100) ML. In the following we focus on the respective magnetic properties of both ML types.

Their magnetic properties appear to be far from trivial. Both geometries have an $\mathrm{AF_I}$ in-plane antiferromagnetic order in their ground state with $\mu_{100}=2.55\mu_B$ and $\mu_{110}=3.30\mu_B$. In the case of Mn(100), the $\mathrm{AF_I}$ magnetic arrangement corresponds at that observed in the (100) planes of δ-Mn in its AF1 ground state. However, it is not the case for the Mn(110) ML for which the $\mathrm{AF_I}$ magnetic arrangement corresponds to the AF2 phase of bulk Mn. This demonstrates *a posteriori* the importance of interlayer hybridization to determine the magnetic order in the bulk phase and suggests a complex behavior for the ML once adsorbed on a substrate. The NM and FM solutions are highly unfavorable. Interestingly our calculations show the existence of two FM states, of low and high spin with $\mu_{100}=1.12/3.95\mu_B$ at equilibrium lattice constants of $a_{100}=2.10/2.60$ Å and $\mu_{110}=1.52/3.86\mu_B$ at $a_{110}=2.60/3.00$ Å. They are almost degenerate for the (110) ML (the energy difference is less than 10 meV/atom) while the low-spin state is slightly more stable by 151 meV/atom for the less compact (100) ML.

The comparison of magnetic and nonmagnetic calculations stresses the large influence of magnetism and its complex correlation with the structure. First of all, taking magnetism into account results in a substantial energy gain reaching 0.29 and 0.51 eV/atom for the (100) and (110) ML upon stabilization of the $\mathrm{AF_I}$ solution. This demonstrates that magnetism is very stable in such low-dimensional nanostructures. Moreover, magnetism can strongly influence the atomic geometry at the energy minimum, indeed, in the nonmagnetic calculations the (100) geometry appears to be more stable than (110) with an energy difference $\Delta E=-0.15$ eV/atom, whereas the stability order is reversed in the spin-polarized calculations with $\Delta E=-0.23$ eV/atom and $\Delta E=-0.28$ eV/atom for the FM and $\mathrm{AF_I}$ solutions, respectively. Furthermore, for each ML geometry the magnetic state strongly affects the equilibrium lattice constant a, Fig. 4 shows that the optimal a for the $\mathrm{AF_I}$ configuration is intermediate between the lattice constants corresponding to the two FM states.

The observed magnetic moments correlate in a very complex manner with the structure and magnetic order that the ML adopt. At fixed lattice constant a, the magnetic moments are generally larger for the less compact (100) ML geometry, which is well understood as the result of the lower atomic coordination leading to a narrower bandwidth. Moreover, at small fixed a the moments within a given geometry are globally larger in the AF solutions than in the FM one. The differences vanish as a increases and at larger a the magnetic moments tend to become equal for both AF and FM solu-

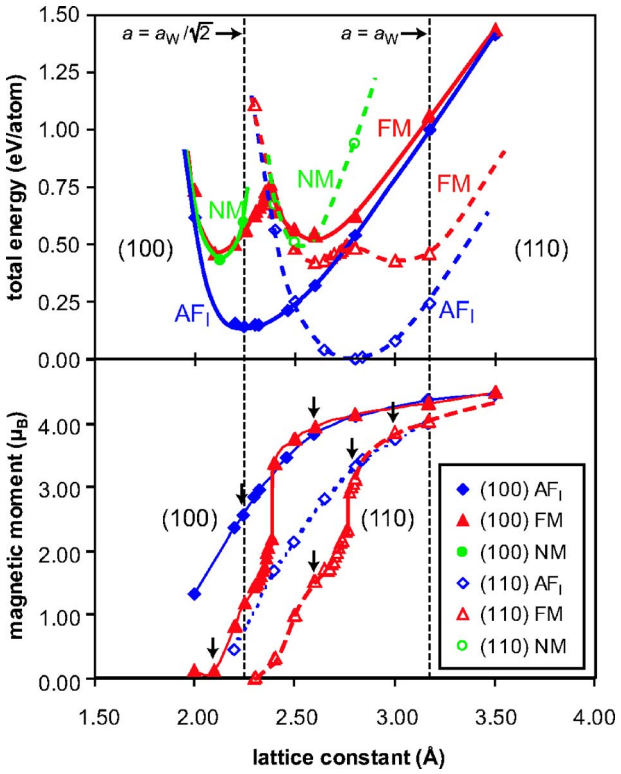

FIG. 4. (Color online) Total energy (top) and atomic magnetic moment (bottom) for (100) and (110) Mn monolayers with different magnetic configurations. The lines are a guide to the eye. The small vertical arrows indicate the magnetic moments at the optimized lattice constant of each configuration. The notations NM, FM, and AF_I stand for the nonmagnetic, ferromagnetic and $c(2\times2)$ in-plane antiferromagnetic solutions, respectively.

tions and for both (100) and (110) geometries, while still remaining below the Hund's rule limit.

In view of the adsorption of thin Mn films on W substrates, it is worth to focus on geometrically constrained Mn ML's whose lattice constant a matches that of the substrate. Figure 5 depicts the different epitaxial systems that we considered in our study. In the case of the pseudomorphic adsorption with $a=3.171$ Å our calculations (see Fig. 4) show that the magnetic moments within both free-standing Mn ML's are almost saturated whatever the magnetic order, with $\mu_{Mn}=4.0$ and $4.3\mu_B$/atom for the (110) and the (100) geometries, respectively. Concerning the stability of the different magnetic orderings, the two ML's behave differently, for the (110) geometry, the AF solution is much more stable by 0.15–0.22 eV/atom than the FM one. Note that the preferred AF_I phase does not correspond to the optimal magnetic order found for bulk Mn strained to match the W(110) surface, therefore, we can conclude this AF_I magnetic arrangement results from the reduced dimension.

On the other hand, for the (100) structure in which the interatomic exchange interactions are weaker due to the increased distances, the different magnetic configurations are almost degenerate with energy differences smaller than 58 meV/atom. These small differences suggest that upon adsorption the hybridization with the substrate will play a dominant role for the determination of the most stable magnetic order, especially in the case of a pseudomorphic Mn(100) ML. On the other hand, the much larger energy differences for Mn(110) are rather in favor of an AF_I order within the adsorbed ML.

As illustrated in Fig. 5, for (100) we also considered the adsorption of a Mn ML with a twice larger coverage according to a $(\sqrt{2}\times\sqrt{2})R45°$ pattern. In this case, the lattice constant of the Mn ML is much smaller, $a=2.242$ Å, which turns out to be very close to the optimal lattice constant of the preferred AF_I magnetic state. At this lattice constant, our calculations show that the energy differences relative to the FM and NM configurations are quite large (about 0.8–0.9 eV/atom). The almost vanishing lattice mismatch between the Mn(100) ML and the W(100) surface seems to suggest the formation of a $(\sqrt{2}\times\sqrt{2})R45°$ overlayer.

IV. STRUCTURE AND MAGNETISM OF THIN Mn/W(100) AND Mn/W(110) FILMS

In this section we first describe isolated Mn atoms adsorbed on clean W(100) and W(110) substrates. Then thin, complete Mn films are considered. The comparison with the preceding section dealing with free-standing Mn ML allows us to discuss the strength of the adlayer-substrate hybridization and the resulting effects on the stability and magnetic properties of the Mn films.

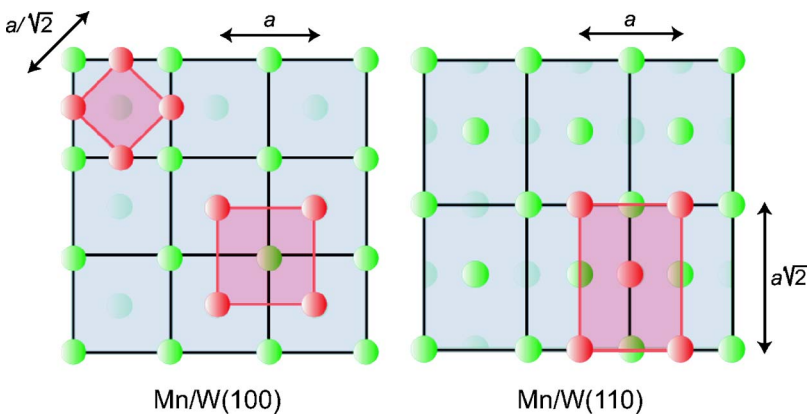

FIG. 5. (Color online) Schematic illustration of the different Mn/W(100) and Mn/W(110) epitaxial systems considered in our study.

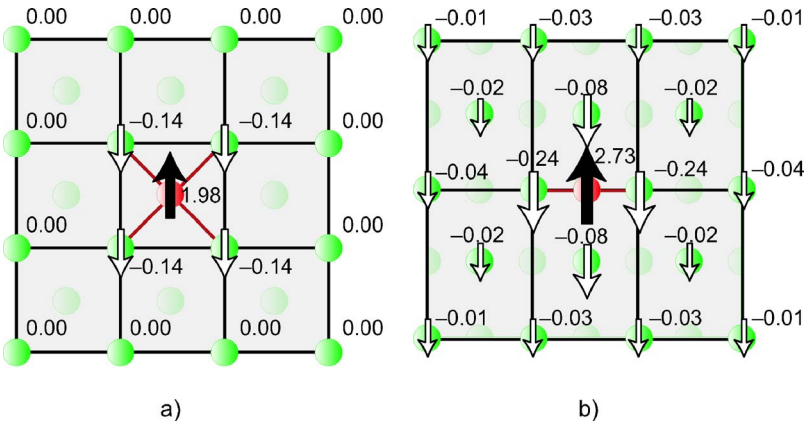

FIG. 6. (Color online) Local magnetic moments for an isolated Mn atom adsorbed on the clean W(100) and W(110) substrates.

A. Isolated Mn atoms adsorbed on W(100) and W(110)

On W(100) the most favorable adsorption site for a Mn atom is the fourfold hollow site as depicted in Fig. 1(b). The adatom located 1.31 Å above the surface induces a modification of the local surface geometry, which locally leads to the vanishing of the surface reconstruction described in Sec. III A. The square geometry characterizing the (100) surface is locally almost recovered with angles of about 85° [to be compared to 78°, see Fig. 1(a)]. The long and short bridge positions at the reconstructed W(100) surface are significantly less stable by 1.06 and 1.16 eV, respectively. These results are a first hint that a pseudomorphic growth of Mn on W(100) can be achieved, at least at a local scale. For sake of simplicity we will consider in the following the nonreconstructed relaxed W substrate [Fig. 6(a)]. In this case, the Mn atom also lies 1.43 Å above the surface in the fourfold hollow. The bridge position represents a transition state for adatom diffusion with an energy increased by 1.23 eV compared to the hollow site.

The case of W(110) is simpler since this surface does not exhibit any surface reconstruction. The Mn adatom prefers staying in the long bridge between two W surface atoms [oriented along the ⟨100⟩ direction, see Fig. 6(b)], at about 1.84 Å above the surface. The short bridge site (along the ⟨110⟩ direction) is less stable by 0.41 eV (the adatom lies 1.99 Å above the surface), while the pseudothreefold hollow turns out to be unstable.

For both (100) and (110) substrates, the Mn adatom retains a quite large magnetic moment of $\mu_{100}=1.98\mu_B$ and $\mu_{110}=2.73\mu_B$, respectively. Note that μ_{110} is higher due to the reduced atomic coordination of Mn in the bridge site. Magnetism has moreover a substantial stabilizing effect as the magnetic solution is more stable by 85 meV and 131 meV than the nonmagnetic Mn/W(100) and Mn/W(110) configurations. As illustrated in Fig. 6, small antiparallel magnetic moments are induced on neighboring W atoms. They amount to about $-0.14\mu_B$/atom for the four W atoms surrounding the Mn atom on W(100), and already vanish for the next-nearest neighbors. For Mn/W(110) the induced moments extend slightly further due to the more compact substrate. Their value for the two W atoms forming the bridge where Mn is adsorbed, $-0.24\mu_B$/atom, is higher due to the reduced coordination.

B. Thin Mn/W(110) films

We begin our discussion of the compact thin Mn films pseudomorphically adsorbed on W substrates by the case of Mn/W(110). Our results are summarized in Table IV.

1. Adsorption process: General tendencies

As shown in Table IV the adsorption is a very highly exothermic process with large adsorption energies. In the following we use adsorption energies defined with respect to the clean nonmagnetic, nonreconstructed, relaxed W surfaces and the free-standing Mn ML with corresponding symmetry and relaxed lattice constant in its AF ground state.

As it is detailed in Fig. 7 for 1 ML thick Mn film, in both magnetic and non magnetic calculations the formation of Mn-W bonds upon adsorption results indeed in a significant energy gain which largely overcompensates the energy cost needed to expand the intralayer Mn-Mn bonds in the ML lattice constant to match the substrate. This suggests a very strong Mn-W hybridization. The interplane distance between the two Mn and W planes at the interface is intermediate between those of bulk W and Mn. For the subsequent Mn overlayers, the inward relaxation is still higher due to the tendency for the Mn atoms to conserve an approximately constant atomic volume despite the large lateral expansion, as already observed in Sec. III B.

Despite the strong hybridization the magnetic behavior of the adsorbed Mn layer is similar to that of the free-standing ML in its ground state, indeed, thin Mn films containing up to three layers pseudomorphically adsorbed on the W(110) substrate adopt AF ground states, while the FM configurations represent metastable solutions of significantly higher energy (for 3 ML Mn films, we were not able to get a converged FM solution) and the NM configurations are highly unfavorable. However, the adsorption generally results in a reduction of the Mn magnetic moments which reaches about $3\mu_B$/atom for the top Mn adlayer and slightly increases with film thickness. At fixed in-plane lattice constant the surface Mn moments in the adsorbed film are intermediate between those of the free-standing constrained ML ($3.99\mu_B$/atom) and those of Mn bulk strained to match the W(110) substrate ($2.84\mu_B$/atom). Smaller Mn moments are calculated for the subsurface and interface layers. Small magnetic moments are

TABLE IV. Adsorption energy E_{ads} (in eV/Mn), change of interlayer distances δ (in %) with respect to the interlayer distance d_{110} =2.24 Å in bulk tungsten, and profile of local magnetic moments μ (in μ_B) relative to the different configurations adopted by thin 1, 2, and 3 ML Mn films adsorbed on the W(110) substrate. The adsorption energy is defined with respect to the optimal Mn(110) ML and the clean ideal relaxed W(110) surface. For each thickness, the relative adsorption energy ΔE_{ads} (in meV/Mn) is given with respect to the most stable magnetic order.

	1 ML Mn/W(110)				2 ML Mn/W(110)						3 ML Mn/W(100)	
	AF_I	AF_{II}	FM	NM	AF_{Ia}	AF_{III}	AF_{II}	AF_{Ib}	FM	NM	AF_{III}	AF_{Ia}
E_{ads}	1.79	1.63	1.60	1.24	1.56	1.52	1.51	1.50	1.40	1.22	1.37	1.36
ΔE_{ads}	0	151	186	512	0	34	47	59	151	335	0	3
$\delta_{II/III}$											−17.8	−14.4
$\delta_{I/II}$					−17.5	−24.6	−18.6	−15.2	−17.5	−37.7	−19.9	−24.2
$\delta_{I/1}$	−6.9	−8.0	−12.2	−17.6	−8.4	−10.7	−10.4	−12.0	−13.0	−7.8	−11.5	−8.8
$\delta_{1/2}$	−0.4	−1.1	−0.2	1.2	−0.6	−0.2	−0.4	0.0	−0.2	−0.8	−0.1	−0.9
$\delta_{2/3}$	0.02	−0.2	−0.3	0.1	0.0	0.0	0.0	0.1	0.1	−0.2	−0.1	−0.9
μ(Mn III)											3.10	±3.55
μ(Mn II)					±3.56	−3.43	±3.51	±3.54	3.49	0.00	−2.96	±1.55
μ(Mn I)	±3.47	±3.31	2.93	0.00	±2.47	1.41	±1.74	±1.81	1.35	0.00	1.27	±1.96
μ(W 1)	±0.26	0.00	−0.24	0.00	±0.18	−0.10	±0.01	±0.09	−0.10	0.00	−0.14	±0.16
μ(W 2)	±0.08	±0.03	0.00	0.00	±0.06	−0.01	±0.01	±0.01	0.01	0.00	−0.04	±0.03
μ(W 3)	±0.03	0.00	0.00	0.00	±0.03	0.00	±0.01	±0.01	0.00	0.00	−0.04	0.00

induced on the few W substrate layers close to the interface, they are in most cases antiparallel to the Mn moments.

2. 1-, 2-, and 3-ML Mn/W(110): Magnetic properties

In a 1 ML thick Mn film, a $c(2\times2)AF_I$ magnetic configuration in which all nearest-neighboring atoms couple antiferromagnetically is by far the most stable, similarly to the free-standing Mn ML of same lattice constant. The adlayer-substrate interlayer spacing, d_{110}=2.09 Å, is almost equal to the average of the corresponding interplane distances in bulk tungsten, d_{110}^{W}=2.24 Å, and in AF bulk δ-Mn strained to match the W(110) substrate, $d_{110}^{str\ Mn}$=1.82 Å (cf. Table II).

The AF Mn magnetic moments are here larger than in the FM configuration (by about 16%) in contrast to the case of the free-standing Mn ML for which the AF_I and FM moments are almost equal. This is correlated to a stronger inward relaxation of the top Mn layer in the FM system, which further increases the hybridization with the substrate. Note that the relaxation is even much larger in the nonmagnetic structure, in agreement with the expected correlation between interatomic distance and magnetic moments.

Between the AF_I and the FM solutions, and close to the latter, we find the $p(2\times1)AF_{II}$ solution. In this case, the magnetic symmetry in the top Mn adlayer leads to zero magnetic moments in the first neighboring W layer.

The present results for 1 ML thick Mn/W(110) films are in good agreement with earlier FLAPW-GGA calculations[27] by Bode *et al.* which predict the same order of the different magnetic arrangements, with similar energy differences (the AF_{II} and FM orders are found 102 and 188 meV/Mn atom higher than the AF_I ground state, respectively). A magnetic moment of $3.32\mu_B$/atom as well as a Mn-W interlayer spacing of 2.14 Å are calculated in the ground state, both values compare well with our findings. Concerning the Mn-W interlayer spacing which is the only parameter directly comparable to the theory that could be measured experimentally, the same authors report a higher experimental value of 2.36 Å. However, they estimate that the agreement between theory and experiment can be considered as quite reasonable since this quantity was derived from STM measurements that introduce an overestimation by about 0.5 Å.

By comparing the results for different geometries and magnetic configurations, it is possible to determine the different contributions to the adsorption energy as presented in Fig. 7. This analysis shows that the adsorption energy is approximately the same in magnetic and nonmagnetic calculations (the difference amounts to only 32 meV/Mn atom), but taking magnetism into account has a large influence on the balance between the different contributions. In nonmagnetic calculations expanding the free-standing ML to make it match the W(110) substrate requires a large energy 1.67 eV due to the large misfit. This is overcompensated by the strong stabilization, by 3.42 eV/Mn atom, resulting from the adsorption at fixed lattice constant. On the other hand, if one assumes an AF_I order, the corresponding contributions have smaller magnitudes, respectively, 0.24 and 2.03 eV/Mn atom. This is mainly due to the larger optimal lattice constant of the AF_I ML needing therefore a smaller expansion to satisfy the epitaxial condition. The formation of an AF_I arrangement starting from the NM free-standing or pseudomorphically adsorbed ML leads to a stabilization by about 0.5 eV/Mn atom, whereas in the expanded ML the energy gain, 1.94 eV/Mn atom, is much higher, in the latter case this is due to the combined factors of reduced coordi-

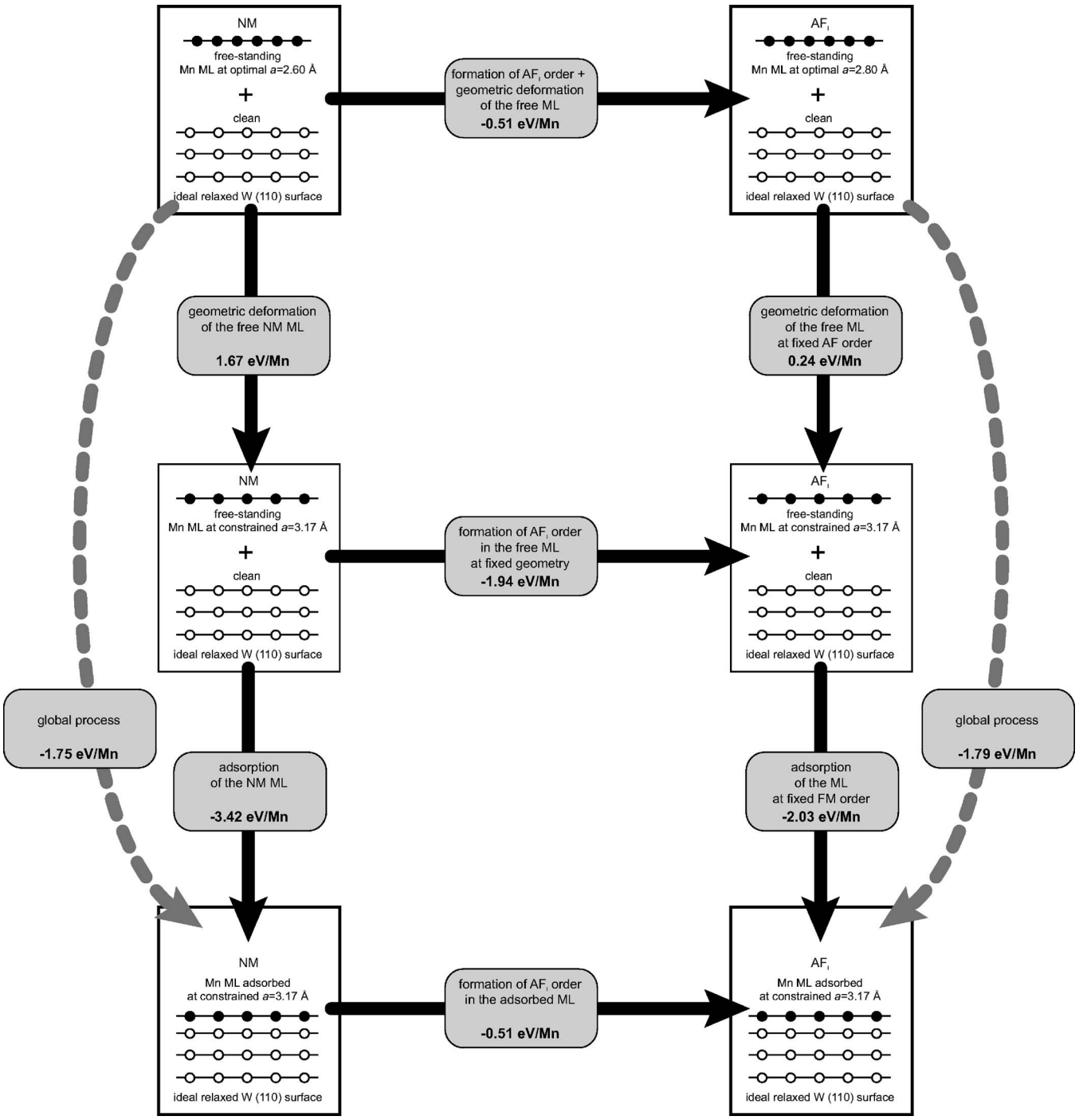

FIG. 7. Different contributions to the adsorption energy in the adsorption process of a pseudomorphic 1 ML Mn film on the nonreconstructed W(110) substrate in nonmagnetic (left-handside) and magnetic calculations (right-handside).

nation and expanded lattice constant which are both favorable to the stabilization of high magnetic moments, whereas in the relaxed free-standing (respectively, adsorbed) ML reduced coordination but small Mn-Mn bond length (respectively, large Mn-Mn bond length but increased coordination due to the hybridization with the substrate) are rather unfavorable to magnetism.

The case of 2 ML thick Mn films is slightly more complex due to the possibility of various AF arrangements. Our notations are explained in Fig. 3. The preferred configuration, that we denote AF_{Ia}, is similar to the case of 1 ML Mn film with a $c(2\times2)$ pattern in each layer. In this arrangement each atom couples antiferromagnetically with its first neighbors in the same plane as well as in the layer right below, leading to vertical (100) planes containing parallel moments. While in the uppermost Mn layer similar magnetic moments as in 1 ML Mn/W(110) are observed, the Mn atoms in direct contact with the W substrate exhibit significantly reduced moments. The substrate polarization is also slightly damped due to the decreased surface influence. From the geometrical point of view, the Mn-Mn layer spacing, $d_{I/II}=1.85$ Å, is already very close to the previously mentioned $d_{110}^{\mathrm{str\ Mn}}$

TABLE V. Energy change $\Delta_{\mathrm{isl}}^{n,h}$ (in meV/surface atom) resulting from the decomposition of a compact $(n+1)$ ML thick Mn film adsorbed on W(110) or W(100) into a compact n-ML thick film covered by h-ML high islands calculated according to Eq. (1).

	On W(110)		On W(100)	
h	$n=0$	$n=1$	$n=0$	$n=1$
2	229	172	450	99
3	420		666	

$=1.82$ Å calculated if one distorts bulk δ Mn to match the W(110) substrate.

A slightly different configuration, AF_{Ib}, has also a $c(2\times2)$ pattern in each layer but shifted in the next layer by $1/2\langle110\rangle$ compared to AF_{Ia}. There, the vertical planes containing parallel moments are the more dense (110) planes and this arrangement is 59 meV/adatom less stable than AF_{Ia}.

It is interesting to note that the first metastable AF configuration (energy difference 34 meV/Mn adatom) is the layer-by-layer AF_{III} arrangement in which all moments in a layer are parallel.

For 3 ML thick Mn films we were able to get only AF_{III} and AF_{Ia} converged solutions, the FM and NM structures being unstable. This stresses the high stabilization of antiferromagnetism in this system. Even if they exhibit quite different magnetic patterns, the two stable AF_{III} and AF_{Ia} arrangements are almost degenerate (energy difference 3 meV/Mn atom). The interlayer spacings, $d_{I/II}=1.80$ Å and $d_{I/II}=1.84$ Å are very close to the spacing calculated for AF bulk δ Mn matching W(110), but the magnetic moments in the central layer turn out to be much smaller. However, our results have shown that a strained δ-Mn crystal matching the W(110) surface has rather a preference for AF1 order (Table II) corresponding in our notations for films to AF_{II} order (Fig. 2), therefore, we can expect that the Mn/W(110) film would converge at higher thickness towards this magnetic arrangement while the hybridization with the substrate locally stabilizes one of the two AF_{III} and AF_{Ia} solutions close to the Mn/W interface. This would however require that such a pseudomorphical growth would be possible at larger thickness. Actually, a stress relieve by formation of misfit dislocations may be rather expected as it was determined for thin Co and Fe films adsorbed on a W substrate.[38]

3. 2D growth vs island formation

These results for compact films at the W surface can give a precious hint to determine a possible tendency to island formation if we assume that islands formed at the surface are sufficiently large so that contributions of edge and side facets to the total energy are negligible. Under this assumption, the energy change per surface unit $\Delta E_{\mathrm{isl}}^{h,n}$ resulting from the decomposition of a smooth Mn film of $(n+1)$ ML into an n-ML thick underlayer and islands with a height of h ML is given by

$$\Delta E_{\mathrm{isl}}^{h,n} = \frac{h-1}{h}E_n + \frac{1}{h}E_{(n+h)} - E_{(n+1)}, \qquad (1)$$

where E_n is the surface total energy of a compact n-ML thick Mn film adsorbed on W in its most stable magnetic configuration. Negative values of $\Delta E_{\mathrm{isl}}^{h,n}$ express favorable conditions for island formation.

From the corresponding formation energies summarized in Table V, one can infer that 1 and 2 ML thick Mn films adsorbed on the W(110) substrate are stable against the formation of higher islands, and this tendency increases with the height of the considered islands. However, the energy cost for island formation is substantially reduced for 2 ML thick films, therefore we can expect that at some height the growth should switch to a growth by islands in order to relieve the stress induced by the large Mn/W misfit.

Our results are in good agreement with experimental conclusions[25,27] of Bode *et al.* who have demonstrated the pseudomorphic growth of Mn films on W(110) up to a thickness of 2 ML. But, since in the experiments even the first Mn layer exhibits a growth anisotropy along the $\langle100\rangle$, one can expect that the edges and side facets should not have a completely negligible influence; currently in progress are further extensive calculations that should clarify this point.

C. Thin Mn/W(100) films

We now discuss in this section the case of thin compact Mn/W(100) films. The experimental results for this substrate are more sparse. There is evidence[28] of a pseudomorphic growth up to a thickness of 15–16 Å but to our knowledge no experimental investigation of magnetism in this system has been performed yet. This stresses the interest of *ab initio* modeling and simulation to supplement the experiments performed in the laboratory.

1. Adsorption process: General tendencies

Our results for 1 ML to 3 ML thick Mn films are summarized in Table VI. For 1 ML thick films, they are completed by Figs. 8 and 9 in which we perform a detailed analysis of the different contributions to the adsorption energy. Since the reconstruction of the clean W(100) surface locally vanishes upon adsorption of a Mn atom, we define here the adsorption energy with respect to the nonmagnetic, nonreconstructed relaxed W(100) surface and the free-standing relaxed Mn(100) ML in its AF ground state. This was further justified by our tests of initially reconstructed Mn/W(100) films that all converged towards nonreconstructed systems.

Similarly to the Mn/W(110), the large adsorption energies (typically 2 eV/Mn atom and higher for the ground state solutions) imply a strong Mn-W hybridization. Like in Mn/W(110), the magnetic moments are reduced compared to the free-standing Mn(100) ML of same lattice constant,

TABLE VI. Adsorption energy E_{ads} (in eV/Mn), change of interlayer distances δ (in %) with respect to the interlayer distance d_{100} = 1.59 Å in bulk tungsten, and profile of local magnetic moments μ (in μ_B) relative to the different configurations adopted by thin 1, 2, and 3 ML Mn films adsorbed on the W(100) substrate. The adsorption energy is defined with respect to the optimal Mn(100) ML and the clean ideal (nonreconstructed), relaxed W(100) surface. For each thickness, the relative adsorption energy ΔE_{ads} (in meV/Mn) is given with respect to the most stable magnetic order.

	1 ML Mn/W(100)					2 ML Mn/W(100)				3 ML Mn/W(100)		
	bcc	bcc	bcc	bcc	bcc R45	bcc	bcc	bcc	1 bcc +1 fcc	bcc	bcc	bcc
	FM	AF_{II}	AF_{I}	NM	NM	FM	AF_{III}	NM	NM	AF_{III}	FM	NM
E_{ads}	2.63	2.56	2.43	2.32	1.50	2.17	2.13	1.86	1.65	1.96	1.86	1.76
ΔE_{ads}	0	63	190	308	1125	0	44	311	514	0	97	194
$\delta_{II/III}$										−20.0	−13.1	−49.2
$\delta_{I/II}$						−6.6	−16.6	−44.7	20.0	−5.4	−21.7	−14.2
$\delta_{I/1}$	−12.5	−16.0	−8.7	−28.9	33.4	−18.5	−7.5	−9.5	−25.5	−12.6	−14.5	−15.6
$\delta_{1/2}$	0.0	0.3	−3.3	4.2	1.0	2.1	−2.0	0.3	2.9	−0.6	0.7	2.1
$\delta_{2/3}$	−0.1	−0.5	0.7	−2.5	−1.0	−1.9	0.1	−1.6	−2.4	−0.5	−0.8	−0.9
μ(Mn III)										3.78	3.71	0.00
μ(Mn II)						3.87	−3.76	0.00	0.01	−3.14	1.34	0.00
μ(Mn I)	3.26	±3.00	±3.44	0.00	0.00	1.31	2.51	0.00	0.01	2.39	1.43	0.00
μ(W 1)	−0.47	0.00	±0.04	0.00	0.00	−0.22	−0.25	0.00	−0.01	−0.34	−0.21	0.00
μ(W 2)	0.10	±0.03	±0.05	0.00	0.00	0.02	0.09	0.00	0.00	0.08	0.03	0.00
μ(W 3)	−0.07	0.00	±0.01	0.00	0.00	−0.02	−0.07	0.00	0.00	−0.07	−0.02	0.00

but generally remain significantly enhanced with respect to bulk δ-Mn strained to match the substrate. At a given magnetic order they are also larger than in Mn/W(110) due to the lower density of the (100) surface. Smaller antiparallel magnetic moments are also induced in the W substrate close to the Mn/W interface. The most remarkable result is the stabilization of FM order in 1 and 2 ML thick Mn films followed by a transition to AF arrangement, as we discuss below.

2. FM 1 ML thick Mn/W(100) films

For 1 ML thick Mn/W(100) films we considered two possible film configurations with different coverages, the pseudomorphic bcc stacking or a configuration according a $(\sqrt{2}\times\sqrt{2})R45°$ pattern with a twice higher coverage. A detailed analysis of the different contributions to the adsorption energy presented in Figs. 8 and 9 turns out to very instructive.

According to Sec. III C, a relaxed free-standing Mn ML has a ground state lattice constant which is almost equal to that of a $(\sqrt{2}\times\sqrt{2})R45°$ film adsorbed on W(100), and thus allows a perfect matching without any geometrical distortion. On the other hand, pseudomorphic growth requires a significant expansion of the ML to make the lattice constants match, which represents a non-negligible energy cost reaching 0.4–0.7 eV/Mn atom in magnetic calculations and up to 3.8 eV/Mn atom in nonmagnetic ones (cf. Table III). However, our results show that the pseudomorphic stacking is by far preferred and generally results in much larger adsorption energies, for both magnetic and nonmagnetic calculations. Following a bond-order argument this can be explained by a weakening of the intralayer Mn-Mn hybridization induced by the adlayer-substrate Mn-W interaction, which tends to put the adlayer under tensile stress. This tensile stress is particularly destabilizing in the case of the $(\sqrt{2}\times\sqrt{2})R45°$ configuration due to the high coverage associated to the conservation of the lattice constant upon adsorption. On the other hand, it has a stabilizing effect on pseudomorphic growth implying a severe expansion of the Mn ML. Note that in this case the Mn-W interlayer spacing (1.39 Å) is about half as large compared to the $(\sqrt{2}\times\sqrt{2})R45°$ stacking (2.11 Å). Moreover, since in the $(\sqrt{2}\times\sqrt{2})R45°$ configuration the higher coordination number is not compensated by an increase of the interatomic distances, magnetism vanishes completely upon adsorption. On the other hand, significant magnetic moments are still present in the Mn films adsorbed pseudomorphically. Altogether, these results demonstrate that the properties of the adlayer-substrate system strongly depend on a subtle balance between intralayer Mn-Mn bonding and film-substrate Mn-W bonding.

From now on, we concentrate on the pseudomorphic pattern which is the most stable one. Like in the Mn/W(110) case, taking magnetism into account in the calculations does not significantly modify the adsorption energy (it results only in a slight increase of 20 meV/atom). However, it leads to a very different balance between the different contributions to the total adsorption energy as illustrated in Fig. 8. In the nonmagnetic calculations, the huge distortion of the nonmagnetic free-standing ML to match the W(100) surface (almost 50%) has a significant cost (3.57 eV/Mn atom) while the adsorption at fixed lattice constant is extremely stabilizing with an energy gain of 5.99 eV/Mn atom. In magnetic cal-

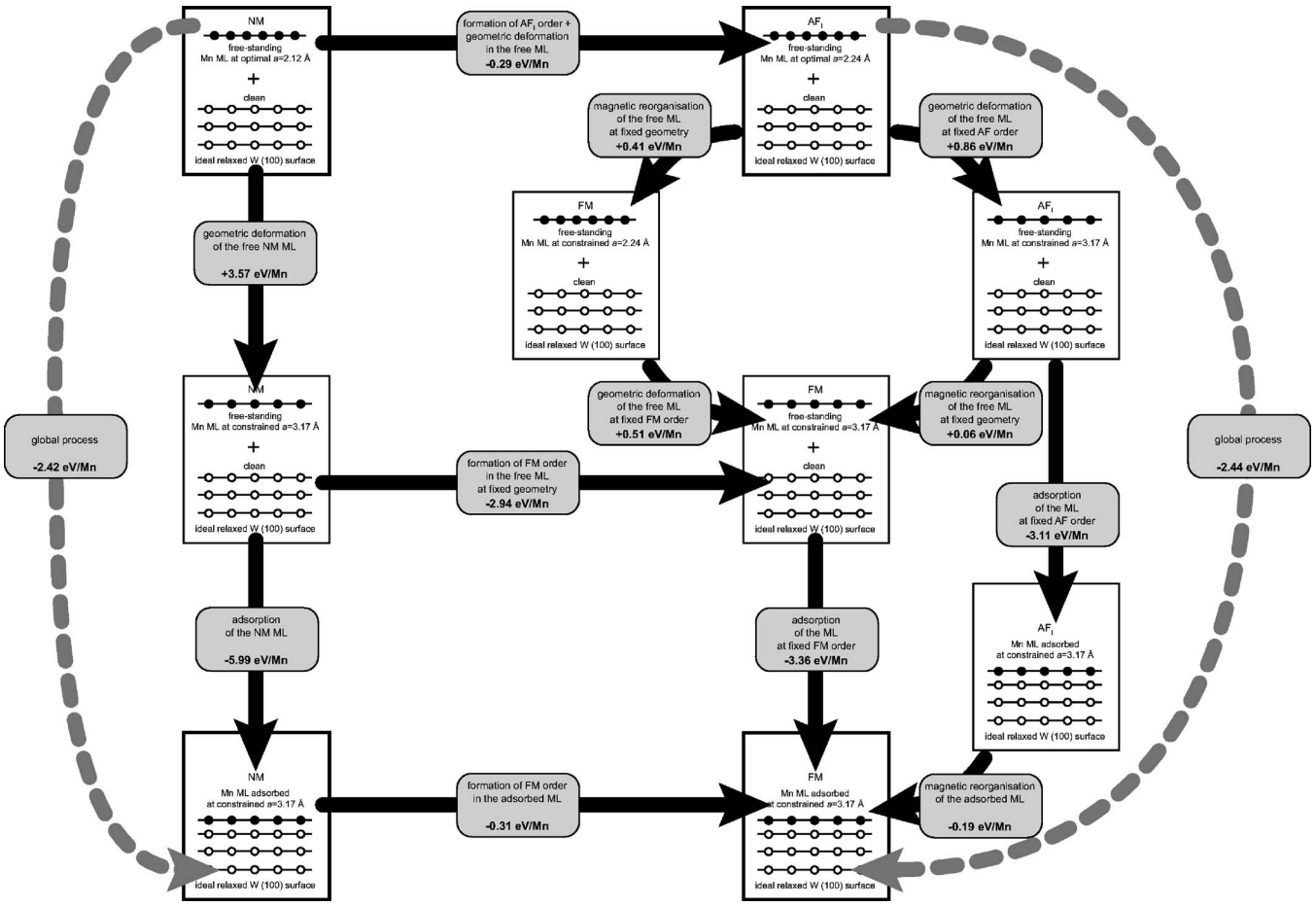

FIG. 8. Different contributions to the adsorption energy in the adsorption process of a pseudomorphic 1 ML Mn film on the W(100) substrate in nonmagnetic (left-handside) and magnetic calculations (right-handside).

culations, the respective contributions are much smaller, the slightly smaller expansion needed to match the substrate (about 40%) results in a substantially reduced destabilizing geometrical contribution to the adsorption energy. The energy gain stemming from the adsorption itself at fixed lattice parameter is also much smaller (3.36 eV/Mn atom if FM order is assumed, 3.11 eV/atom if AF_I). The energies needed to modify the magnetic order from AF to FM or vice versa within the free-standing or adsorbed ML are much smaller (of the order of a few 100 meV/Mn atom). Note that the magnetic energy difference between the NM ML in its relaxed free-standing geometry (low coordination number but small lattice constant) or pseudomorphically adsorbed structure (larger lattice constant but higher coordination number) at the FM ground state is not particularly stabilizing with an energy gain of only about 0.3 eV/Mn atom, while the stabilization is much more significant when the free-standing ML is expanded to match the W substrate (energy gain of 2.94 eV/Mn atom) since in this case magnetism is highly favored due to both reduced coordination and large lattice constant.

From the magnetic point of view, the existence of FM order in monolayer films of the antiferromagnetic metal Mn on W(100) substrates is very surprising—in particular as a free-standing Mn-ML has an antiferromagnetic ground state, irrespective of its geometry (see Sec. III C and Eder *et al.*[29]). This demonstrates that the FM ground state is due solely to hybridization with W atoms. The energy difference between AF and FM arrangements amounts to 63–190 meV/Mn atom in Mn/W(100), i.e., it is much higher and of opposite sign than for the free-standing ML of the same lattice constant (absolute energy difference 12–58 meV/Mn atom). The individual Mn atoms carry large parallel magnetic moments, $3.26\mu_B$/atom, of the same order as in Mn/W(110) and should be easily detected by local experimental techniques like Mössbauer spectroscopy. After the prediction of AF ordering in monolayer films and nanostructures of the ferromagnetic metals Fe and Co on tungsten substrates [1 ML Co/W(110) films, Fe-Co monowires adsorbed on steps of a W(970) substrate,[38] 1 ML Fe/W(110) films[39]] this is another important of a substrate-induced change of magnetic order in nanostructures.

3. 2 and 3 ML thick Mn/W(100) films: Transition towards AF order

Figure 10(a) illustrates the most stable adsorption site for an isolated Mn atom adsorbed on a 1 ML Mn/W(100) film, as well as the local magnetic moments. Mn adatom is preferentially accommodated on the fourfold hollow site, i.e., according to a pseudomorphic growth. Its high magnetic

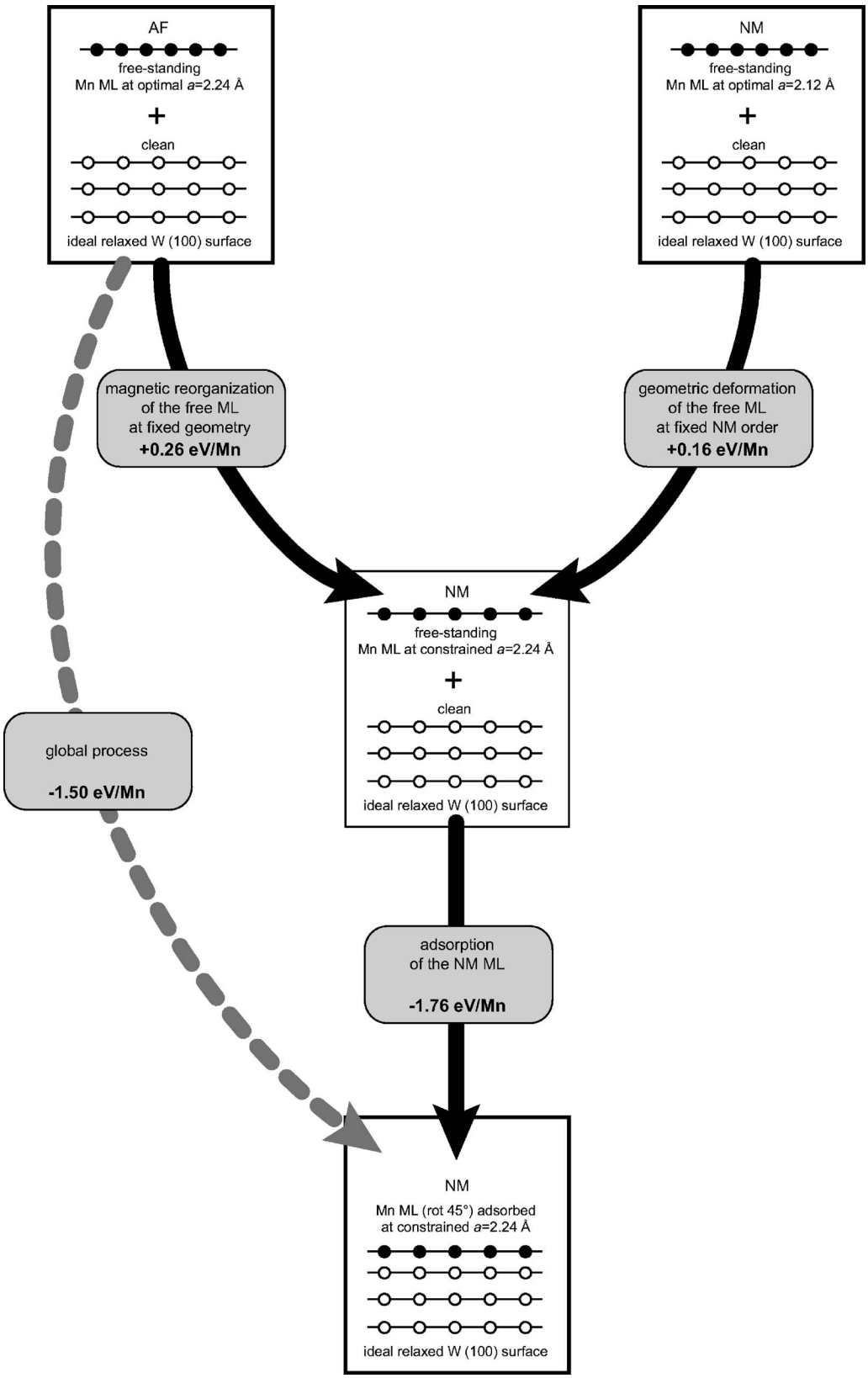

FIG. 9. Adsorption process of a nonpseudomorphic $(\sqrt{2}\times\sqrt{2})R45°$ 1 ML Mn film on the W(100) substrate.

moment resulting from the reduced coordination couples ferromagnetically with the Mn underlayer, but locally leads to a small decrease of the magnetic moments ($2.7\mu_B$/atom against about $3.0\mu_B$/atom far from it).

In complete 2 ML Mn/W(100) films the same FM picture is conserved with enhanced moments of $3.87\mu_B$/atom in the uppermost layer. In this case, we could not make in-plane AF solutions converge. Instead, a metastable AF_{III} solution

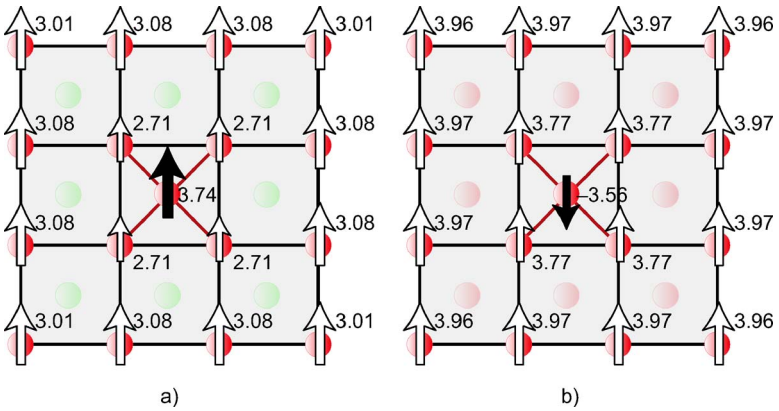

FIG. 10. (Color online) Local magnetic moments for an isolated Mn atom adsorbed on a 1 ML Mn/W(100) film (left-handside) and on a 2 ML Mn/W(100) one (right-handside), in the most favorable hollow sites.

(where the Mn moments couple ferromagnetically in each plane, but where the two Mn layers are coupled antiferromagnetically) is found to be 44 meV/Mn atom higher in energy. In 1 ML films the energy difference between FM and in-plane AF solutions was slightly larger, 63–190 meV/Mn atom.

We also examined the possibility of a slightly different atomic arrangement in the capping Mn layers, with a pseudomorphic bcc layer first and a fcc-like layer on top of it. But this configuration was found to be nonmagnetic and highly unprobable compared to the 2 ML thick pseudomorphic films.

Since it has been shown that the FM order results solely from the hybridization with the W substrate, a transition can be easily expected towards one of the AF structures which are much more favored in bulk Mn strained to fulfill the epitaxial matching conditions. Our calculations presented in Table VI demonstrate that this transition occurs already for 3 ML thick films, which suggests that the influence of the W substrate extends only over a rather short length scale of about 2 ML. Indeed the preferred configuration in 3 ML thick films is the AF_{III} structure which is 97 meV/Mn atom more stable.

However, since it implies the flipping of all moments of the second layer, the FM-AF transition should to be rather slow with increasing Mn coverage. Figure 10(b) presents the change of the local moments induced by an isolated Mn atom adsorbed on a FM 2 ML thick Mn film. In contrast to a Mn adatom on 1 ML Mn/W(100) [Fig. 10(a)], the adatom on 2 ML Mn/W(100) couples antiferromagnetically with the underlayers. It leads only to a local decrease of the magnitude of the other Mn moments. Therefore we can expect that a minimal size of Mn islands adsorbed on 2 ML Mn/W(100) is needed to make the magnetic order switch from FM to AF_{III}.

4. 2D growth vs island formation

Similarly to our discussion of Sec. IV B 3, these results can be used to predict a possible tendency to island formation. From the total energy calculated for the most stable 1, 2, and 3 ML thick Mn/W(100) films, the energy cost for the decomposition of a compact film into a underlayer with formation of islands was determined, as summarized in Table V. Like Mn/W(110) films, the Mn/W(100) films seem to have a preference to form smooth films: this trend is quite pronounced for a single Mn with large formation energies of 2 ML and 3 ML high islands of more than 450–666 meV/surface atom. However, for 2 ML thick Mn films the formation energy of 2 ML high islands is strongly reduced (99 meV/surface atom). Therefore, after sufficient deposition of Mn the system should probably switch to island formation to minimize the large tensile stress induced by epitaxial conditions.

V. CONCLUSIONS AND OUTLOOK

We have presented an extended first-principles DFT investigation of the structural and magnetic properties of thin Mn films deposed on W substrates. In good agreement with experiments,[25–28] pseudomorphically adsorbed Mn films up to three ML are found to be thermodynamically stable despite the large tensile strain induced by the epitaxial conditions. For a single Mn ML on W(110), the adlayer-substrate spacing compares favorably with the experimental value. The analysis of the large adsorption energies has revealed a complex balance between destabilizing elastic effects resulting from the large expansion needed to match the W lattice and the stabilization stemming from the strong Mn-W hybridization. Magnetism does not change the adsorption energy significantly but substantially modifies the respective magnitudes of the different contributions.

For Mn/W(110) our results demonstrate a $c(2\times2)$ in-plane AF order for thicknesses up to 3 ML, with a degenerate layered antiferromagnetism in the (110) planes for 3 ML thick Mn/W(110) films. This is in agreement with recent experiments[26,27] that demonstrated the existence of this AF superstructure by spin-polarized STM imaging at low temperature. In spite of the strong hybridization, large magnetic moments of about $3.5\mu_B$/atom are still sustained by the Mn atoms, while smaller antiparallel moments are induced on the substrate atoms in the vicinity of the interface.

For Mn/W(100) our calculations predict a FM arrangement in 1 and 2 ML thick films whose origin is the sole hybridization with the substrate. Large magnetic moments of 3.3 to almost $4\mu_B$/atom are calculated for the surface Mn atoms. The stabilization of ferromagnetism in the Mn ML is driven by two effects, (i) the strong reduction of the magnetic energy difference on expansion, and (ii) the large ad-

sorption energy for an expanded ML with a FM instead of a AF configuration, caused by a strong Mn/W hybridization across the interface. Between 2 and 3 ML, a transition to an antiferromagnetism layered in (100) planes is predicted. Since this transition involves the flipping of the magnetic moments in the entire second Mn layer, one can expect the existence of a critical Mn island size or Mn coverage during the formation of the third layer needed to switch from FM to AF. Mn/W(100) films are a third example—after Fe/W(100) and Co/W(110)—for a change in the magnetic ground state in a two-dimensional film relative to the bulk material induced by adsorbate-substrate interactions. Interestingly, the present case of Mn/W(100) films where ferromagnetism replaces antiferromagnetism is opposite to that of Fe/W(100) and Co/W(110) films, for which a previous studies[38,39] predicted AF order (instead of FM like in the bulk) for a single ML and a transition to FM order at thicknesses higher than 2 ML. This confirms the importance of the hybridization with the substrate to determine the magnetic properties of thin films, and in particular it stresses the necessity to carefully choose the substrate to properly adjust their properties.

Finally, the magnetic contribution to the adsorption has been determined by comparing magnetic and nonmagnetic calculations. The comparison of the results obtained for the thin adsorbed films with results calculated for bulk δ Mn and free-standing Mn ML in the same theoretical formalism has allowed to estimate the effects induced by the reduced dimensionality.

In the following paper,[55] the studies of the static and magnetic properties of Mn/W films will be extended to the investigation of atomic diffusion in these systems, with the aim to achieve a better insight in the growth mechanism of the films.

Note added in proofs. After this work was submitted, Ferriani *et al.* published a comparative theoretical study[56] of 3*d* transition-metal single ML adsorbed on W(100) in which they also reported a FM order for a 1 ML thick Mn film. However, the calculated adlayer-substrate interlayer distances appear smaller in their work [FM, -4.7%, $c(2\times2)$ AF, -0.8%] compared to the present one [FM, -12.5%, $c(2\times2)$ AF, -8.7%]. The high accuracy of our calculations was carefully checked through extensive convergence studies and is supported by the careful analysis of the surface relaxations of the clean W(110) and W(100) surfaces—the excellent agreement with both other *ab initio* calculations and with experiment is documented in Sec. III A as well as in previous work of our group.[39] Rather, the origin of the discrepancies should be found in the different computational setups. Ferriani *et al.* used the experimental lattice parameter of the W substrate, whereas all our calculations have been performed for the theoretical lattice parameter. Moreover, in Ref. 56 only the distance between the adlayer and the substrate was relaxed, whereas we performed a full multilayer relaxation of the adlayer-substrate system. The difference between the theoretical and experimental lattice constants, as well as the relaxation of the W substrate, are modest, but since the W-W binding is so much stronger than the Mn-W binding, this is the most likely explanation of the discrepancies. The argument used in Ref. 56 to explain the surface relaxation based on a a full majority and an empty minority band holds only for the trend across the series of 3*d*-films on W(100), but not for the absolute values of the relaxation. For understanding the magnitude of the relaxation effects, arguments related to the conservation of the local atomic volume seem to be much more important.

ACKNOWLEDGMENTS

This work has been supported by the EU Commission within the STREP Project "Dynamics in Nano-Scale Materials" (Contract No NMP4-CT-2003-001516). The calculations were performed on Schrödinger II computer system at the Computer Center of Vienna University.

*Email address: samuel.dennler@univie.ac.at

[1] *Frontiers in Surface and Interface Science*, edited by C. B. Duke and E. W. Plummer (North-Holland, Elsevier, Amsterdam, 2002). See in particular the papers by S. D. Bader (p. 172), D. T. Pierce, J. Unguris, R. J. Celotta, and M. D. Stiles (p. 290), J. Shen and J. Kirschner (p. 300), A. Fert and L. Piraux (p. 338), R. H. Kodama (p. 359), E. E. Fullerton, J. S. Jiang, and S. D. Bader (p. 392), F. J. Himpsel, K. N. Altmann, G. J. Mankey, J. E. Ortega, and D. Y. Petrovykh (p. 456), and by I. K. Schuller, S. Kim, and C. Leighton (p. 571).

[2] For a review on the GMR effect see, e.g., J. Nogues and I. K. Schuller, J. Magn. Magn. Mater. **192**, 203 (1999).

[3] H. A. Dürr, E. Duzik, S. S. Dhesi, J. B. Goedekopp, G. van der Laan, M. Belakhovsky. C. Mocuta, A. Marty, and Y. Samson, Science **284**, 2166 (1999).

[4] A. Scholl, J. Stöhr, J. Lüning, J. W. Seo, J. Fompeyrine, H. Siegwart, J. P. Locquet, F. Nolting, S. Anders, E. E. Fullerton, M. R. Scheinfein, and H. A. Padmore, Science **287**, 1014 (2000).

[5] H. Zabel, J. Phys.: Condens. Matter **11**, 9303 (1999).

[6] W. B. Pearson, *A Handbook of Lattice Spacings and Structures of Metals and Alloys* (Pergamon, Oxford, 1958).

[7] D. Hobbs, J. Hafner, and D. Spišák, Phys. Rev. B **68**, 014407 (2003).

[8] J. Hafner and D. Hobbs, Phys. Rev. B **68**, 014408 (2003).

[9] Y. Endoh and Y. Ishikawa, J. Phys. Soc. Jpn. **30**, 1614 (1971).

[10] T. Oguchi and A. J. Freeman, J. Magn. Magn. Mater. **46**, L1 (1984).

[11] J. Hafner and D. Spišák, Phys. Rev. B **72**, 144420 (2005).

[12] J. Kübler, J. Magn. Magn. Mater. **20**, 107 (1980).

[13] V. L. Moruzzi, P. M. Marcus, and P. C. Pattnaik, Phys. Rev. B **37**, 8003 (1988).

[14] S. Fujii, S. Ishida, and S. Asano, J. Phys. Soc. Jpn. **60**, 1193 (1991).

[15] Y. Nishihata, M. Nakayama, N. Sano, and H. Terushi, J. Phys. Soc. Jpn. **63**, 319 (1988).

[16] W. F. Egelhoff, I. Jacob, J. M. Rudd, J. F. Cochran, and B.

Heinrich, J. Vac. Sci. Technol. A **8**, 1582 (1990).
[17] M. Wuttig, Y. Gauthier, and S. Blügel, Phys. Rev. Lett. **70**, 3619 (1993).
[18] M. Wuttig, B. Feldmann, and T. Flores, Surf. Sci. **331–333**, 659 (1995).
[19] D. Tian, S. C. Wu, F. Jona, and P. M. Marcus, Solid State Commun. **70**, 199 (1989).
[20] S. Andrieu, H. M. Fischer, M. Piecuch, A. Traverse, and J. Mimault, Phys. Rev. B **54**, 2822 (1996).
[21] B. Heinrich, A. S. Arrott, C. Liu, and S. T. Purcell, J. Vac. Sci. Technol. A **5**, 1935 (1987).
[22] T. G. Walker and H. Hopster, Phys. Rev. B **48**, R3563 (1993).
[23] S. K. Kim, Y. Tian, M. Montesano, F. Jona, and P. M. Marcus, Phys. Rev. B **54**, 5081 (1996).
[24] Y. Tian, F. Jona, and P. M. Marcus, Phys. Rev. B **59**, 12647 (1999).
[25] M. Bode, M. Hennefarth, D. Haude, M. Getzlaff, and R. Wiesendager, Surf. Sci. **432**, 8 (1999).
[26] S. Heinze, M. Bode, A. Kubetzka, O. Pietzche, X. Nie, S. Blügel, and R. Wiesendanger, Science **288**, 1805 (2000).
[27] M. Bode, S. Heinze, A. Kubetzka, O. Pietzsch, M. Hennefarth, M. Getzlaff, R. Wiesendanger, X. Nie, G. Bihlmayer, and S. Blügel, Phys. Rev. B **66**, 014425 (2002).
[28] Y. Tian and F. Jona, J. Phys.: Condens. Matter **13**, 1805 (2001).
[29] M. Eder, J. Hafner, and E. G. Moroni, Phys. Rev. B **61**, 11492 (2000).
[30] D. Spišák and J. Hafner, J. Phys.: Condens. Matter **11**, 6359 (1999).
[31] S. L. Qiu, P. M. Marcus, and Hong Ma, J. Appl. Phys. **87**, 5932 (2000); Phys. Rev. B **62**, 3292 (2000).
[32] U. Gradmann and G. Waller, Surf. Sci. **116**, 539 (1982).
[33] H. J. Elmers, J. Hauschild, and U. Gradmann, Phys. Rev. B **54**, 15224 (1996).
[34] H. Knoppe and E. Bauer, Phys. Rev. B **48**, 1794 (1993).
[35] M. Pratzer, H. J. Elmers, and M. Getzlaff, Phys. Rev. B **67**, 153405 (2003).
[36] W. Wulfhekel, F. Zavaliche, R. Hertel, S. Bodea, G. Steierl, G. Liu, J. Kirschner, and H. P. Oepen, Phys. Rev. B **68**, 144416 (2003).
[37] G. Garreau, M. Farle, E. Beaurepaire, and K. Baberschke, Phys. Rev. B **55**, 330 (1997).
[38] D. Spišák and J. Hafner, Phys. Rev. B **70**, 014430 (2004).
[39] D. Spišák and J. Hafner, Phys. Rev. B **70**, 195426 (2004).
[40] A. Kubetzka, P. Ferriani, M. Bode, S. Heinze, G. Bihlmayer, K. von Bergmann, O. Pietzsch, S. Blügel, and R. Wiesendanger, Phys. Rev. Lett. **94**, 087204 (2005).
[41] M. Pratzer and H. J. Elmers, Phys. Rev. B **69**, 134418 (2004).
[42] G. Kresse and J. Hafner, Phys. Rev. B **47**, R558 (1993).
[43] G. Kresse and J. Furthmüller, Phys. Rev. B **54**, 11169 (1996); Comput. Mater. Sci. **6**, 15 (1996).
[44] P. E. Blöchl, Phys. Rev. B **50**, 17953 (1994).
[45] G. Kresse and D. Joubert, Phys. Rev. B **59**, 1758 (1999).
[46] H. J. Monkhorst and J. D. Pack, Phys. Rev. B **13**, 5188 (1976).
[47] E. G. Moroni, G. Kresse, J. Hafner, and J. Furthmüller, Phys. Rev. B **56**, 15629 (1997).
[48] A. Eichler, J. Hafner, and G. Kresse, J. Phys.: Condens. Matter **8**, 7659 (1996).
[49] J. P. Perdew, K. Burke, and M. Ernzerhof, Phys. Rev. Lett. **77**, 3865 (1996).
[50] P. Villars and L. D. Calvert, *Pearson's Handbook of Crystallographic Data for Intermetallic Phase*, 2nd ed. (ASM International, Materials Park, Ohio, 1991).
[51] J. P. Perdew, J. A. Chevary, S. H. Vosko, K. A. Jackson, M. R. Pederson, D. J. Singh, and C. Fiolhais, Phys. Rev. B **46**, 6671 (1992).
[52] S. H. Vosko, L. Wilk, and M. Nusair, Can. J. Phys. **58**, 1200 (1980).
[53] M. S. Altman, P. J. Estrup, and I. K. Robinson, Phys. Rev. B **38**, 5211 (1988).
[54] R. Yu, H. Krakauer, and D. Singh, Phys. Rev. B **45**, 8671 (1992).
[55] S. Dennler and J. Hafner, following paper, Phys. Rev. B **72**, 214414 (2005).
[56] P. Ferriani, S. Heinze, G. Bihlmayer, and S. Blügel, Phys. Rev. B **72**, 024452 (2005).